**RADAR RESPONSE OF LUNAR CRYPTOMARIA AND PYROCLASTIC DEPOSITS IN MINI-RF DATA.**

A. M. Bramson[1], L. M. Carter[1], G. W. Patterson[2], and M. M. Sori[1]. [1]Lunar and Planetary Laboratory, University of Arizona (bramson@lpl.arizona.edu), [2] Johns Hopkins University Applied Physics Laboratory

**Introduction:** Quantifying the volumes and nature of (e.g. explosive vs. effusive) lunar volcanic eruptions is important for constraining the thermal and geologic evolution of the Moon, as well as the evolution of volatiles in the lunar interior. The distribution of cryptomare and pyroclastic deposits each provide crucial pieces to the puzzle of understanding the spatial and temporal history of volcanism on the Moon. Pyroclastic deposits are characterized by low albedo, smooth mantling units that formed due to explosive eruptions from volatile-enriched magma reservoirs [e.g., 1]. Meanwhile, cryptomaria are effusive, basaltic lava flows from early in lunar history that were subsequently buried by higher-albedo basin/crater ejecta [e.g., 2].

The Schiller-Schickard region is one of the most established sites of cryptomare due to a combination of spectral mixing analyses [3–5], dark halo craters and nearby geologic context [6–8], and gravity signatures [9]. Radar wavelengths, and their ability to probe the near-subsurface, offer the opportunity to investigate vertical spatial scales in between those probed by surface spectra and the deeper signs of cryptomaria associated with gravity anomalies. Radar has also proved to be a useful tool for identifying pyroclastic deposits which may not be apparent in optical images, but appear radar dark in same-sense circular polarization echoes due to the nature of the fine-grained material and lack of blocky material [e.g., 10].

**Methods:** Mini-RF is a hybrid-polarized, side-looking synthetic aperture radar (SAR) onboard NASA's Lunar Reconnaissance Orbiter (LRO), which was designed to transmit a circularly polarized signal and receive both orthogonal linear polarizations [11]. The system was built as a monostatic system, however, the transmitter malfunctioned in 2010. This precipitated the development of a new bistatic architecture in which ground-based assets transmit a signal (Arecibo Observatory for S-band, $\lambda$=12.6 cm, and the Goldstone deep space communications complex 34-meter antenna DSS-13 for X-band, $\lambda$=4.2 cm) to illuminate a portion of the lunar surface, and Mini-RF's receiver intercepts the backscattered signal [12]. This set-up allows for radar scattering properties of the Moon to be measured as a function of bistatic angle (a phase angle for radar wavelengths), which would not have been possible in Mini-RF's original monostatic, phase angle 0º, configuration.

Here, we measure Stokes parameter $S_1$ (total backscattered power of the wave), same sense polarization (SC; depolarized signal), opposite sense polarization (OC; specular reflection), and circular polarization ratio (CPR; a ratio of SC/OC) across areas of interest in the monostatic and bistatic datasets.

For the monostatic data, we used the geospatial information system *JMARS (for the Moon)* [13] to "sample" these radar properties across four terrains – highlands, mare, pyroclastic deposits and cryptomaria. For the highlands and mare, we exported the Mini-RF pixels within five 10-km-diameter circles scattered across representative terrain to give us control values for these already-well-characterized terrains. Additionally, we sampled three regions of known pyroclastic units: Aristarchus, Taurus Littrow, and Rima Bode, and three regions of known/suspected cryptomaria: Schiller-Schickard, Balmer, and Hercules. The putative mare deposits in each of these cryptomare regions are thought to be buried by a different amount of basin/crater ejecta [8]. We took measurements of the Mini-RF data binned to 16 ppd resolution as to increase the signal-to-noise of the data. We computed the mean and standard deviation in each of our five remote-sensing "samples" for each of the 8 terrains/regions of interest listed above. Then we propagate the mean and standard deviations through for the five samples to obtain our average measurement for that particular terrain/ROI.

We compare the monostatic data to the bistatic radar responses in Mini-RF data, where available, across these terrains to look for similarities within terrain types as well as differences between different units of the same terrain-type. 70-cm Arecibo data have been used to map cryptomaria east of Orientale basin, which exhibit low radar returns due to the underlying mare's effect on the bulk loss tangent [14]. We will look for a consistent radar signature in Mini-RF data associated with cryptomaria, which can then be used to look for new, smaller-scale deposits that may either be (a) too deep to exhibit the surface spectral signatures, or (b) too small to be detectable by GRAIL gravity data. We compare the radar response of cryptomaria to pyroclastic deposits and control sites of mare and highlands material to investigate the similarities and differences between these geologic units' radar signatures, and their relationship to other datasets (Titanium content, Clementine color ratios, etc). Such a holistic, comparative study will allow us to model and characterize how these volcanic units interact with radar waves, and facilitate more precise mapping of explosive (pyroclastics) and buried effusive (cryptomare) volcanism on the Moon.

**Preliminary Results and Discussion:**

*Mini-RF Monostatic Data:* As expected, we find that the pyroclastic units exhibit lower backscattered returns

(Figure 1). This is consistent with smooth mantling units that lack wavelength-sized roughness and scatterers. The CPR for the units in Taurus Littrow and Rima Bode are higher than that at Aristarchus, and appears to be correlated to higher $TiO_2$ abundances at these locations (Figure 2), suggesting their low-backscatter behavior may be partly compositional.

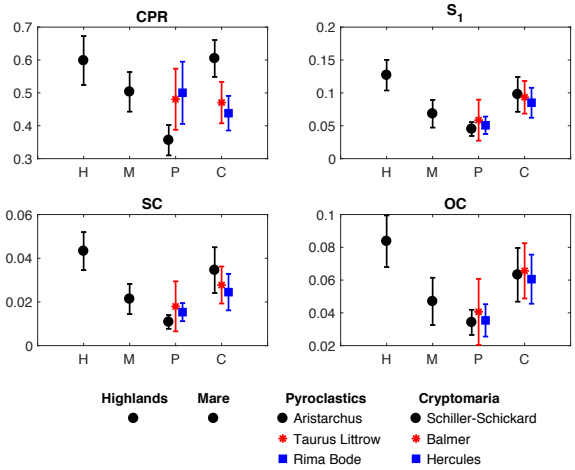


*Figure 1: Comparison of radar properties across four terrains, including three regions of interest of pyroclastic deposits and cryptomaria.*

The backscattered power from the cryptomaria regions are intermediate between the mare and highlands control values (Figure 1), consistent with a near-subsurface consisting of both mare and highlands materials. The CPR of Schiller-Schickard is higher than the other cryptomaria regions investigated here, and is similar to that of the highlands. This CPR suggests that this cryptomaria unit may be buried deeper such that the radar signal is dominated by scattering due to the superposition of rougher, cratered highlands material. This interpretation is consistent with spectral analyses, which found a strong mixture of mare and highland materials only around deep excavation spots, like dark-halo craters, whereas the rest of the region generally only showed weak mixtures of basalt [5]. All three cryptomaria regions exhibit low $TiO_2$ abundances to high certainty (Figure 2), which suggests differences between these three regions are due to the roughness and blockiness at cm and m scales in the near-subsurface rather than absorptive titanium at the surface.

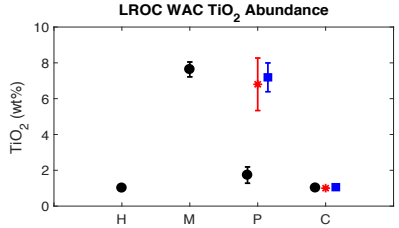


*Figure 2: $TiO_2$ abundances from LROC WAC data in the same "samples" as Figure 1.*

*Mini-RF Bistatic Data:* We also measured the CPR and $S_1$ as a function of bistatic angle across six S-band observations of pyroclastic deposits, two in the area of Aristarchus and four observations at Littrow D, as well as a comparative measurement of the crater ejecta blanket at Byrgius A (Figure 3). The Aristarchus measurements yield flat backscatter signatures with respect to bistatic angle, consistent with results in [12]. We will analyze the additional bistatic observations that are available to characterize pyroclastics and cryptomaria, particularly to inspect lower bistatic angles for an opposition peak at 0° phase angle, which may differentiate terrain based on roughness and composition [12, 15, 16].

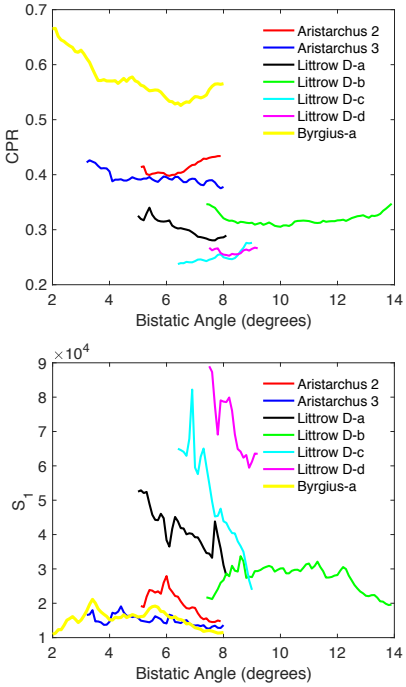


*Figure 3: CPR and total backscatter power $S_1$ as a function of bistatic angle.*

**References:** [1] Gaddis et al. (1985) *Icarus, 61*, 461–489. [2] Antonenko et al. (1995) *Earth, Moon, Planets, 69*, 141–172. [3] Mustard et al. (1992) *LPSC 23*, 957–958. [4] Head et al. (1993) [5] Hareyama et al. (2019) *Icarus, 321*, 407–425. [6] Schultz and Spudis (1983) *Nature, 302*, 233–236. [7] Hawke et al. (1985) *Earth, Moon, Planets, 32*, 257–273. [8] Whitten and Head (2015) *Icarus, 247*, 150–171. [9] Sori et al. (2016) *Icarus, 273*, 284–295. [10] Carter et al. (2009) *JGR, 114*, E11004. [11] Raney et al. (2011) *Proc. of IEEE, 99*, 808–823. [12] Patterson et al. (2017) *Icarus, 283*, 2–19. [13] Christensen et al. (2009), *AGU Fall Meeting*. [14] Campbell et al. (2005) *JGR, 110*, E09002. [15] Piatek et al. (2004) *Icarus, 171*, 531–545. [16] Hapke et al. (2012) *JGR, 117*, E00H15.